Ion transport in macroscopic RF linear traps

Jofre Pedregosa-Gutierrez, C Champenois, Marius Romuald Kamsap, Martina Knoop

Ion transport in macroscopic RF linear traps

Jofre Pedregosa-Gutierrez,* Caroline Champenois,
Marius Romuald Kamsap, and Martina Knoop
Aix-Marseille Université, CNRS, PIIM, UMR 7345,
Centre de Saint Jérôme, 13397 Marseille Cedex 20, France

(Dated: July 18, 2014)

Abstract

Efficient transport of cold atoms or ions is a subject of increasing concern in many experimental applications reaching from quantum information processing to frequency metrology. Different transport schemes have been developed, which allow to move single atoms minimizing their energy gain. In this work, the experimental implementation of the transport of an ion cloud in a macroscopic linear radiofrequency (RF) trap is discussed. Numerical simulations done by molecular dynamics are carried out, which take into account realistic experimental potentials in order to design a method to shuttle large ion samples in a very short time. The deformation of the trapping potential and the spatial extension of the cloud during transport appear to be the major sources for the energy gain of the ions. The efficiency of transport in terms of transfer probability and ion number is also discussed.

PACS numbers: 37.10.Ty (Ion trapping) 37.10.Rs (Ion cooling) 06.30.Ft (Time and frequency)

* jofre.pedregosa@univ-amu.fr

I. INTRODUCTION

Since the very first experiments of guided ion beams by radiofrequency (RF) electric fields [1], transport is a relevant issue in experiments involving trapped ions. For many different applications it is important to shuttle ions from one trap to another, the main conditions being the absence of heating of the atoms and the maximization of the transported ion number. Ion transport has become a standard item in mass spectrometry experiments, where it is often coupled to external ion creation, by various techniques reaching from Electrospray Ionization (ESI) (see for example [2]) to the production of exotic ions at CERN [3]. In most of these experiments, the efficiency of transport has to be high, without necessarily reaching 100 %. In some situations, the use of buffer gas increases performances as it damps eventual heating. Different geometries of linear RF guides can be used, where quadrupole and octupole geometries are the most popular ones.

Recent advances in quantum information processing, in particular the different realizations of scalable architectures [4] rely on the transport of single ions. The transport in this case has to be made with an extremely high fidelity [5], faster than adiabatic for decoherence reasons, and with the ion remaining in the vibrational ground state [6],[7]. Furthermore, ensembles of cold neutral atoms have been shuttled making use of shortcuts to adiabacity [8, 9].

In many experimental situations, speed of operation can be an issue. We are interested in frequency metrology issues for larger clouds of trapped ions similar to [10, 11], and to that purpose, we have recently build a multi-trap system combining two macroscopic linear traps : one of quadrupole and one of octupole geometry [12]. Our objective is to study ion dynamics for various potentials, and the device relies on shuttling ions along a common z-axis. In the case described below, adiabatic transport of the sample would require transfer times of several tens of seconds, which is at least an order of magnitude longer than the interrogation times, and constitutes a dead time in the overall experiment, which we would like to reduce.

In the present work we use numerical simulations to explore the dynamics of the ions during the transport process as it provides access to many parameters, and allows to prepare the experiment. Our aim is to explore the vast parameter regime in order to identify the most robust and efficient way to shuttle an ion cloud between several traps. Throughout this paper we use the parameters of our set-up in order to describe a given case; nevertheless general conclusions will apply to a multitude of set-ups. Clouds of up to 1000 ions are shuttled in a double linear quadrupole trap of overall length of $l = 50$ mm, $r_0 = 3.93$ mm, segmented by three DC-electrodes. Our simulation realistically describes the ions in their environment, by taking into account all relevant forces (trapping potential, Coulomb interaction) as well as laser-cooling as a stochastic process. The mechanical effect of light is implemented by momentum kicks induced by photon absorption and emission, like described in [13, 14]. Trap potentials can be described either analytically or by directly making use of the SIMION po-

tential grid [15] which reproduces the experimental geometry of the electrodes. Throughout this paper, we use the calcium ion mass and the standard experimental parameters of our set-up within the quadrupole part[12], for the molecular dynamics simulations. Such trap geometry is representative of a typical macroscopic implementation of a linear RF trap.

The manuscript is organized as follows. We first review the transport of an ion cloud in an ideal translated harmonic potential. In section III, we introduce the constraints and limits induced by the experimental implementation of the transport in a macroscopic trap designed for large clouds, followed by the study of the transport in a realistic double trap potential, as given by SIMION. In the last subsection, the transport efficiency is discussed in terms of the initial number of trapped ions.

II. ION TRANSPORT BY TRANSLATING A HARMONIC POTENTIAL

A. Center-of-mass motion

In the limit case where ions are trapped in a harmonic potential, the CM of an ion cloud follows the same dynamics as a single ion [16], and therefore this behavior is investigated as a first approach of the ion cloud transport. In the ideal case where the ions can be transported by translating a stationary harmonic potential characterized by a constant eigen-frequency ω_0 and a moving minimum, $z_{min}(t)$, the trapping potential can be written as

$$U_0(t) = \frac{1}{2} m\omega_0^2 (z - z_{min}(t))^2 \tag{1}$$

where m is the mass of the ion. In the following, different time profiles are used to describe the particular temporal evolution of the potential minimum, $z_{min}(t)$.

Assuming an ion initially at rest at the equilibrium position, the final energy of the ion after a transport of duration t_g, can be obtained analytically [17] by introducing a generalised kinetic energy $E(t_g) = m|\Xi(t_g)|^2/2$ which depends on the acceleration of the potential minimum along the transport:

$$\begin{aligned} |\Xi(t_g)|^2 = &\left(\int_0^{t_g} \cos(\omega_0 t) \ddot{z}_{min}(t) dt \right)^2 \\ &+ \left(\int_0^{t_g} \sin(\omega_0 t) \ddot{z}_{min}(t) dt \right)^2 . \end{aligned} \tag{2}$$

This expression connects the transferred energy to the Fourier transform of the force pushing the ion, at frequency ω_0. It can serve as a figure of merit to compare different time profiles, like done in [17, 18] where three different shapes of potential-minimum time profiles are compared, which stand for different characteristic behaviour of the initial, final, and average acceleration. More recently, Torrontegui *et al.* designed a polynomial profile for fast

transport without heating based on the dynamical invariants associated to the Hamiltonian [19].

In the present work, the energy gain, induced by transport protocols following the four mentioned potential-minimum time profiles, is compared for a single ion in a 1D potential and the CM of a cloud in a 3D potential. The general expression for these time profiles is

$$z_{min}(t) = f_i(t)(H(t) - H(t - t_g)) + LH(t - t_g) \tag{3}$$

with $H(t)$ the Heaviside step function and f_i, one of the analytic profiles listed below, with $s = t/t_g$ the relative duration and L the shuttling distance :

$$f_{lin}(s) = Ls \tag{4}$$

$$f_{sin}(s) = \frac{L}{2}\left(1 - \cos\left(\pi s\right)\right) \tag{5}$$

$$f_{tanh}(s) = \frac{L}{2}\left(\frac{\tanh(2N_H s - N_H)}{\tanh(N_H)} + 1\right) \tag{6}$$

$$f_{poly}(s) = L\Big(\frac{60s - 180s^2 + 120s^3}{t_g^2\omega_0^2} + 10s^3 - 15s^4 + 6^5\Big) \tag{7}$$

The impact of the N_H coefficient of Eq.(6) is analyzed in [18] and we choose $N_H = 4$ throughout this paper as a compromise between a linear (N = 1) and a step function ($N \to \infty$). The polynomial profile designed in [19] is the only one which depends explicitly on the considered harmonic potential. The final energy of a single ion shuttled by each of these time profiles can be analytically derived as a function of the oscillation phase during the shuttling $\theta = \omega_0 t_g$.

The final energy for the hyperbolic tangent case is plotted on figure 1 (a) and compared with the polynomial case (b). The evolution profiles share the same features : a decreasing envelope for the maximum energy gain, and a periodic cancellation of the energy gain related to the frequency of the harmonic oscillation of the potential. The hyperbolic tangent profile is the only one giving rise to a behaviour with two different time scales, already noticed in [18] : the periodic cancellation appears only for a minimum value of θ, which depends on the chosen N_H. For shorter shuttling times, the energy gain reaches very high values and decreases drastically as a function of duration. For longer shuttling times, the envelope shows a continuous decrease that is faster than that of the other three profiles. On long time scales, a comparison of the expected energies show that the hyperbolic tangent profile seems to be the most advantageous choice for transport without heating.

In many situations the ion is not in the potential ground state and therefore has non-null initial velocity, as for example for an ion which is only laser-cooled to the Doppler limit. In this case, the final energy can be obtained by integrating the equation of motion, including the force derived from the moving harmonic potential of Eq.(1). When initializing the ion at the potential minimum with a kinetic energy corresponding to an energy of 1 mK and its velocity vector oriented towards the shuttling destination, we observe no

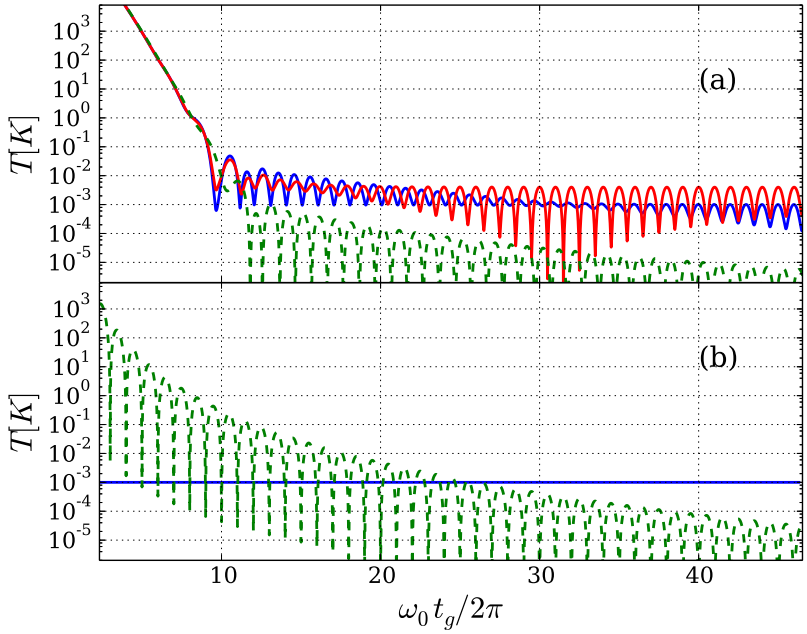

FIG. 1. (Color online) Time evolution of the total energy (in Kelvin) of a single ion after transport over a distance of 23 mm for (a) a hyperbolic tangent time profile (Eq. 6), and (b) a polynomial time profile (Eq. 7). The green dashed lines follow the analytical expression (Eq. 2). The behaviour changes if the ions are initialized with a non-zero energy, as can be observed on the blue curves (initial velocity equivalent to an energy of 1 mK), or red curves (4 mK).

major differences for the linear and sinusoidal profiles, except for the values of the periodic minima: while the linear profile results in a periodic cancellation of the energy gain, the sinusoidal function cancels the total energy. This difference can be of importance in single ion shuttling experiment if the ion's energy needs to be reduced.

In the case of a polynomial time profile, the final energy completely looses its periodic features and equals exactly the initial energy. Actually, this profile has been designed for an immobile start and arrival [19], it is very robust against a non-zero initial velocity and no energy gain was observed in the velocity range we explored. On the other hand, shuttling with a hyperbolic tangent profile still shows a final energy with a periodic structure. For short enough shuttling duration, the minimum energy equals the initial energy whereas after a few tens of oscillation periods, the final energy after shuttling is reduced below the initial value. The exact duration for possible energy loss depends on the initial velocity of the ion: the larger the initial velocity, the shorter the shuttling duration must be to attain energy reduction.

B. Ion cloud transport

As demonstrated in [16] for two ions, the motion of the CM of an ion cloud is expected to follow the dynamics of a single ion if the translated potential is harmonic. Extending this analogy to a cloud of N_0 ions with Coulomb repulsion requires to consider the dynamics in 3D. In a first step, we choose the trapping potential in an ideal RF linear quadrupole trap:

$$\begin{aligned}\Psi(t,x,y,z) &= (V_{DC} - V_{RF}\cos(\Omega t))\tfrac{x^2-y^2}{r_0^2} \\ &+ \tfrac{1}{2}m\omega_0^2\left[(z - z_{min}(t))^2 - \tfrac{x^2+y^2}{2}\right] \end{aligned} \quad (8)$$

We set the trap parameters in the adiabatic regime [20] with a Mathieu parameter $q_x = 0.14$ (V_{RF} = 250 V, $\Omega/2\pi$ = 5.25 MHz for r_0 = 3.93 mm). V_{DC} is fixed at 1 V, a value too small to modify the potential depth but sufficient to prevent the cloud rotation observed in this kind of simulation in axially symmetric potentials [14]. In the adiabatic approximation, the radial oscillating potential is equivalent to a harmonic static potential characterized by $\omega_x/2\pi = 281$ kHz. Furthermore, we choose for ω_0 a value which leads to an aspect ratio R/L of the ion cloud in the cold limit equal to 0.31, which corresponds to a 3D morphology with a cigar shape [21, 22]. This implies that $\omega_0/2\pi = 124$ kHz and the effective radial harmonic potential is given by $\omega_r = 267$ kHz. Such values correspond to our experimental set-up as described in [12].

Before shuttling, the initial conditions of the ion cloud is prepared in three steps : first, the ions are set at random positions following a Gaussian distribution, and with zero velocity. From this moment on, they experience the trapping force and the Coulomb repulsion. After 100 RF periods, where no cooling is applied, the thermal bath technique is used: at a time for which the RF-driven velocity is null, the ion velocity is periodically re-scaled in the three directions such as to reach a temperature of the ensemble equal to $T_{bath} = 1$ mK to within a 1% precision [23]. Finally, the thermal bath is turned off and the ions are submitted to laser Doppler cooling for an evolution time of 5 ms. In our case, the laser beam propagates along the trap symmetry axis, which is sufficient to cool the ion cloud in the three degrees of motion because of its 3D morphology [14]. We treat the atomic system as a two-level atom and chose laser interaction parameters in the slightly saturated regime (s=1.5 for a detuning corresponding to 2.5 times the natural linewidth) which allows the velocity distribution to reach an equilibrium corresponding to a temperature $T \approx 4$ mK. With the chosen trapping parameters, the phase transition to a Coulomb crystal is expected to happen at 5 mK, if we use the condition demonstrated for the bulk [24]. As most simulations imply only 100 ions, this transition is expected to happen for a lower temperature. The important fact here is that the kinetic energy of the ions is negligible compared to the Coulomb repulsion rather than the structural state. The laser cooling is kept during the transport but we estimated that its role is negligible, as the Doppler effect induced by the transport shifts the ions out of resonance.

The dynamics simulations show that, once the transport completed, the CM oscillates with an amplitude depending on the transport duration. To have an estimation comparable with the total energy of a single ion, like given by Eq.(2), the maximum value taken by the CM velocity during the last six oscillations is selected to compute the equivalent temperature. Moreover, the shuttling is expected to induce some discrepancies between the kinetic energy in the radial and axial directions, we have therefore calculated both of them separately, T_r^{CM}, T_z^{CM}.

As expected, the energy transferred to the CM of the ion cloud during transport closely follows the one for a single ion, except for very low $\omega_0 t_g/2\pi$ (a few oscillations). The simulations have also confirmed that Torrontegui's polynomial profile offers a major advantage as the energy gain cancellation regime does not require specific transport durations and can theoretically be operated for times shorter than one oscillation period. Experimental realizations of this transport without energy gain, have to make sure that the translated harmonic potential remains constant. While this can be closely reproduced in micro-fabricated traps, it seems unrealistic to achieve such a feature in macroscopic set-ups, simply due to the scale and the reduced number of electrodes of these traps. In the following, we show the limitations introduced by the experimental realization in macroscopic traps and how they modify the ion cloud heating.

III. EXPERIMENTAL IMPLEMENTATION

The practical realization of an ion-cloud transport is based on the time variation of the voltages applied to the electrodes used for the axial confinement. We call such a voltage variation a waveform. In order to determine the required waveform, two approaches are found in the literature concerning single-ion shuttling. The first one is to search for waveforms which keep the axial trapping potential as close as possible to a harmonic potential with a constant secular frequency throughout the transport. This approach can be found in [25], where a constrained least-squares optimization algorithm is used to transport an ion in a X junction and in [6, 7] for transport along a linear multizone trap, where the electrodes are sufficiently close to keep the local potential unchanged.

An alternative to achieve heating without transport consists in using optimal control theory as done in [26]. In this approach, the algorithm output is a waveform that minimizes the ion's phase space displacement after the transport. What happens during the transport itself is not relevant (even if constraints can be imposed). Simulations based on the control theory require to solve the equations of motion as many times as required until the algorithm converges. This is computationally feasible for a small number of ions, but for a large ion cloud, the Coulomb interaction is too costly in calculation time to consider such an approach.

The above cited examples of shuttling within a well controlled potential were designed in micro-fabricated traps where the typical distance covered by the ion is of the order of

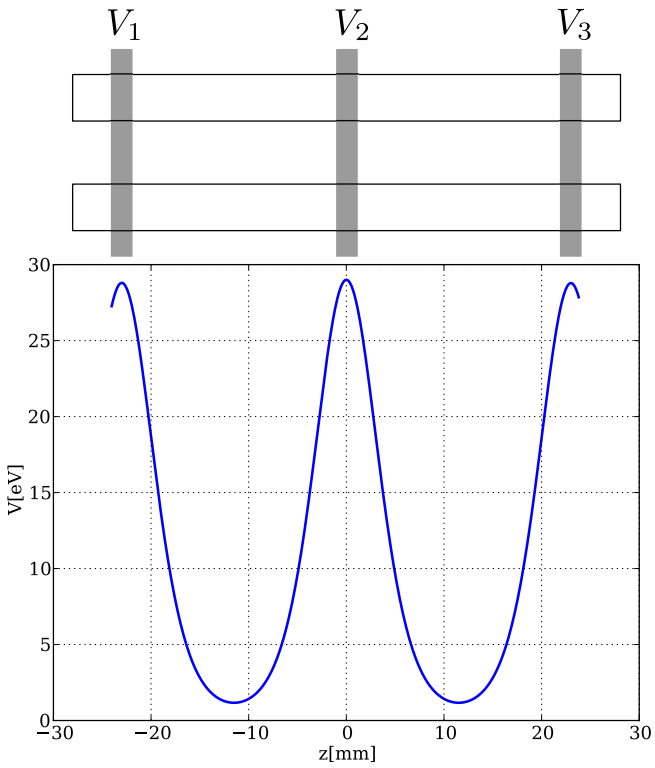

FIG. 2. (Color online) Top : Schematic drawing of the double trap. Gray: DC electrodes, white: RF electrodes. Bottom : Axial potential generated by 1000 V applied to the DC electrodes.

few 100 μm thanks to the variation of the voltage applied to a number of electrodes ranging from 4 to 78, with a large size compared to the covered distance. In our experiment, the transport distance for the ion cloud is 23 mm along an RF quadrupole trap split in two trapping zones by a 2 mm wide extra DC-electrode, setting to 3 the number of available electrodes. Regarding dimensions and external control parameters this is more comparable to the macroscopic set-ups used in mass spectrometry [2], but without the damping role of buffer gas and with the objective of a fast and 100 % efficient shuttling. In the next subsections, we address the issue of the design of the waveforms, as well as their impact on the ion cloud final energy and ion number after transport.

A. Design of waveforms for ion transport

We now focus on the feasibility of a successfully transport performed with the three electrodes present in [12], the smallest number of electrodes available. Figure 2 shows the trap sketch including the potential distribution and notations. If we call $\phi_i(x, y, z)$ the electric potential created by electrode i when 1V is applied to it, the total DC potential

inside the trap can be expressed as [27]

$$\Phi(t,x,y,z) = \sum_{i}^{N} V_i(t)\phi_i(x,y,z) \tag{9}$$

if $V_i(t)$ is applied to electrode i. In the following, the dependence on x and y is neglected due to the small size of the cloud with respect to the radial size of the trap, therefore $\phi_i(x,y,z)$ can be written as $\phi_i(z)$.

Building a harmonic potential centered on the moving $z_{min}(t)$ implies that

$$\frac{\partial \Phi}{\partial z}\Big|_{z_{min}(t)} = 0 \tag{10}$$

$$\frac{\partial^2 \Phi}{\partial z^2}\Big|_{z_{min}(t)} = \frac{m\omega_0^2}{Q} \tag{11}$$

where Q is the ion charge. Equation (10) leads to :

$$V_2(t) = -\frac{V_1(t)\phi_1^{'}(z) + V_3(t)\phi_3^{'}(z)}{\phi_2^{'}(z)}\Big|_{z_{min}(t)} \tag{12}$$

where $\phi_i'(z)$ is the first order derivative relative to z. Depending on the shape of the electrodes, the $\phi_i(z)$ function can take different forms but they always show a maximum at the center of the electrode which implies that $\phi_2'(z_2) = 0$ if we call z_2 the center of the second electrode. For any combination of $V_1(t)$ and $V_3(t)$, Eq (12) leads to a discontinuity of $V_2(t)$ when $z_{min}(t) = z_2$. One can avoid this discontinuity by imposing a constant relation between $V_1(t)$ and $V_3(t)$ given by

$$V_3(t) = V_1(t)\frac{\phi_2'\phi_1'' - \phi_1'\phi_2''}{\phi_3'\phi_2'' - \phi_2'\phi_3''}\Big|_{z=z_2} \tag{13}$$

which simplifies to $V_3(t) = -V_1(t)\phi_1'(z_2)/\phi_3'(z_2)$ if one assumes $\phi_2'(z_2) = 0$, which may not be satisfied in a simulation where the space variables are discretized, as needed in the following. Indeed, the more general expression given by Eq.(13) allows the cancellation of the discontinuity even if the space grid does not match exactly the center of the second electrode. Furthermore, in a perfectly symmetric device where the central electrode splits the trap in two identical trapping zones, $\phi_1'(z_2) = -\phi_3'(z_2)$ leading to $V_3(t) = V_1(t)$. Any asymmetry in the electrode environment breaks this equality and the ratio $V_3(t)/V_1(t)$ has to be modified in order to cancel the discontinuity.

In the trap we consider here, the potential $\phi_i(z)$ generated by each electrode has a FWHM of 3.9 mm which is far smaller than the distance between electrodes, equal to 23 mm (cf. Figure 2). Huge and unrealistic voltages are then required to obey Eq.(11). To overcome this impossibility, we study the effect of the deformation of the potential along the transport where the only effective control concerns the position of the potential minimum. In practice, the ratio V_3/V_1 is kept constant and chosen to cancel the discontinuity and $V_2(t)$ is designed such that $z_{min}(t)$ follows the chosen time profile. To have a realistic diagnostic, the molecular

dynamics simulation of the cloud is carried out inside the potential generated from the real experimental geometry as given by SIMION8.1 [15]. The same potential is used to compute V_3/V_1 and $V_2(t)$. To study the effects of the non-stationarity of the potential along the transport, we look first at the behaivour on a single ion as a representation of the CM. Afterwards, results concerning the ion cloud will show how the spatial extension of the ion cloud plays an important role in the final energy.

B. Energy gain

1. The CM motion

The energy of the axial motion of the cloud's CM just after its transport is plotted on figure 3 for two cases: transport in the full potential and transport in the harmonic part of this potential. These two curves are compared with the energy of a single ion transported in the full potential. The single ion starts at the potential minimum with an initial velocity equivalent to an energy of 1 mK, oriented towards the transport destination. The transport duration is still expressed in terms of a harmonic oscillation period $2\pi/\omega_0$ where ω_0 is deduced from the second derivative of the total axial potential at the beginning of the transport $\omega_z(t=0)$ with

$$\omega_z^2(t) = \frac{Q}{m}\frac{\partial^2\Phi}{\partial z^2}\Big|_{z_{min}(t)} \tag{14}$$

The comparison of these three curves first shows that, for the four tested potential minimum time profile (Eq.(4-7)), the energy gain of the CM motion has the same behavior as the single ion case, provided that only the harmonic contribution to the axial potential is kept. This behavior is characterized by a net increase of the CM energy, induced by the transport. The periodic minima of the energy gain observed for the translated harmonic potential are now washed out, except for the linear case, for which a double period is observable. Except for these periodic minima, the final energy is several orders of magnitude higher than the initial one, showing a drastic increase of energy. All simulations show a decreasing final energy with longer transport duration, the lowest-lying energy curve is obtained for the sinus profile.

The origin of the several orders of magnitude energy increase in the deformed harmonic potential is to be looked for in the difference in the potential evolution compared to the translated harmonic potential transport : the spatial profile of the potential changes along the transport, resulting in an effective $\omega_z(t)$ which is plotted on figure 4 for the four potential minimum time profiles.

As long as a single ion is concerned, the molecular dynamics simulation run in a harmonic potential with the time varying secular frequency given by 14 show the same features as the one run in the full potential $\Phi(t,x,y,z)$. This demonstrates that the cause of the transport

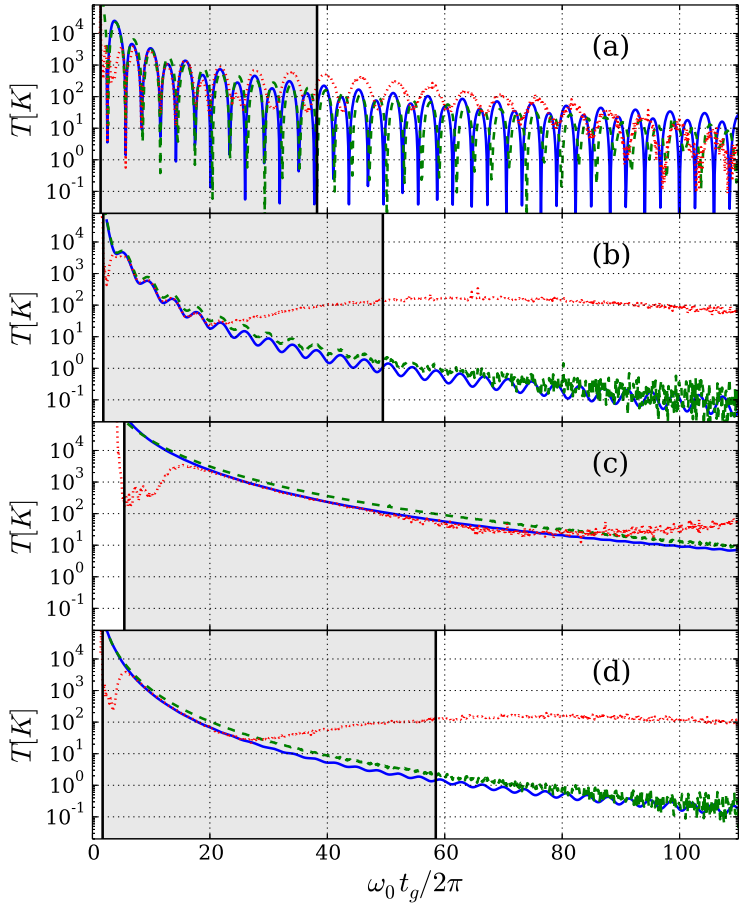

FIG. 3. (Color online) Axial motion energy of the CM of a 100-ion cloud transported in the full 3D moving potential like described in III A (red dotted line), versus the transport duration in reduced units $\omega_0 t_g/2\pi$. For comparison, the dashed green lines show the results for the same cloud when only the harmonic contribution of the axial potential is kept (see Eq.(14)), and the single ion case is indicated by the solid blue line. The different minimum time profiles obey a linear (a), a sinus (b), a hyperbolic tangent (c) and a polynomial function (d). The shaded areas indicate the duration for which 100% of the ions are transported.

induced energy gain of a single ion is the time variation of the harmonic component of the potential, the extra terms having only a very small influence. The preservation of the periodic minima for the linear case may be explained by its kinetic effect. In practice, a linear profile results in a kick forward at the beginning of the transport and a kick backward at its end resulting in a smaller sensitivity to the intermediate evolution.

The calculated $\omega_z(t)$ shown on figure 4 for the four chosen time profiles all reach a value three orders of magnitude smaller than the initial one, at half transport duration, which in practice corresponds to a potential minimum located at the central electrode. This feature prevents the design of an adiabatic transport scheme for such a set-up. Indeed, the

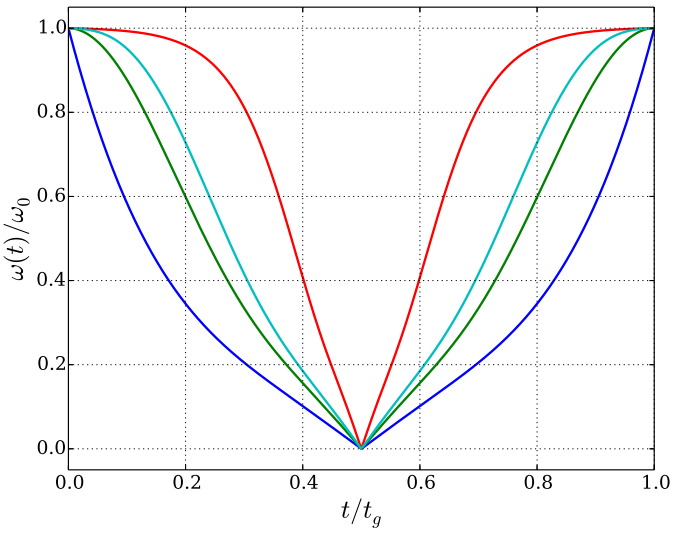

FIG. 4. (Color online) Relative time evolution of the effective $\omega_z(t)$ versus the relative transport duration t/t_g, like calculated with Eq.(14) for the potential-minimum time profile following a linear (blue), a sinus (green), a hyperbolic tangent (red) and a polynomial function (cyan).

adiabaticity criteria for a time varying secular frequency $\omega_z(t)$ without transport is given by $\dot{\omega}/\omega^2 < 1$. Due to our trap geometry and trapping parameters, this condition leads to transport durations of 5 s to 60 s, depending on the chosen transport profile. The time evolution of $\omega_z(t)$ calculated for the sinus and polynomial time profiles are very close, which could explain why the energy gain of the axial motion of CM (see Figure 3) behaves similarly for these two cases, showing very close orders of magnitude for all the tested transport duration.

The comparison in figure 3 shows that when the simulations are run in the full potential, the CM energy split from the one calculated in its harmonic contribution (except for the linear profile) when the energy in the CM motion reaches a value of the order of 40 K, which happens for very different transport durations. This increase of the final energy of the CM makes long transport inappropriate for ion clouds, except with a linear profile (which presents other drawbacks presented in section III C). The role of the higher order terms in the full axial potential is analyzed in the following.

2. Impact of the spatial spreading of the cloud

Studies of the spatial spreading of the cloud along its transport explain why higher order terms in the full axial potential play a role for long transport durations. This is shown on Figure 5, where the maximum distance between the CM and an ion is plotted for a cloud made of 100 ions and 1000 ions. For each cloud, we have chosen two characteristic

durations for transport by a sinus time profile : one for which the numerical simulations give approximately the same final energy for the full and harmonic potential ($t_g = 100$ μs, $\omega_0 t_g/2\pi = 12.4$ for N_0=100 and N_0=1000) and one which results in very different final energy ($t_g = 400$ μs, $\omega_0 t_g/2\pi = 49.6$ for N_0=100 and $t_g = 250$ μs, $\omega_0 t_g/2\pi = 31.0$ for N_0=1000). First, we observe that the spreading of the cloud during its transport is very

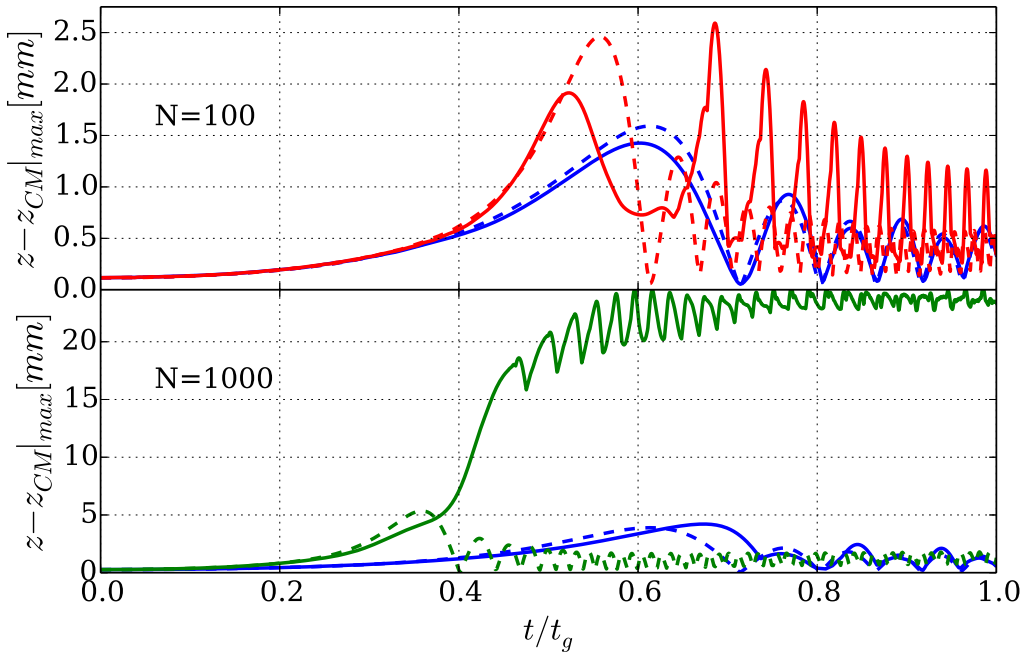

FIG. 5. (Color online) Spatial extension (largest value of $z_i - z_{CM}$) of a 100-ion cloud (a) and a 1000-ion cloud (b) transported in the full 3D moving potential (solid lines) and in its harmonic contribution (dashed lines), versus relative time (t/t_g), for durations of 100 μs (blue lines), 250 μs (green) and 400 μs (red). The potential-minimum time profile obeys a sinus function.

similar in the full potential and in its harmonic contribution for $t_g = 100\mu$s. The oscillations are the signature of the cloud breathing around its CM. The maximum amplitude is reached by the first breathing which happens around 60% of t_g. The situation is very different for the 400 μs and 250 μs duration, where the breathing starts relatively sooner and the breathing in the full potential is rapidly out of phase with the one observed in the harmonic potential, leading to a larger ion cloud spread (≈ 2.5 times in the $N_0 = 100$ case and ≈ 12.5 for the $N_0 = 1000$). For a large spatial extension of the cloud, some ions experience a part of the axial potential which is far from harmonic and it is known that non-harmonic terms are responsible for coupling between internal and CM degrees of motions. Nevertheless, the energy gain on CM motion is far larger than the one observed on the kinetic energy in the CM frame called internal energy in the following.

The evolution of the axial internal energy can be resumed as follows. In case of a transport

in the full potential, the axial internal kinetic energy reaches values as large as 10000 K for short transport durations. For long enough transport, it fluctuates around a mean value of 100 K, reached at different t_g for different time profiles : 50 μs for the sinus and polynomial functions, to 200 μs for the linear and tanh functions. If only the harmonic contribution of the potential is kept, even the shortest transports result in a mean axial internal kinetic of 100 K for any of the t_g and time profile studied.

Concerning the radial internal kinetic energy, no drastic heating is observed for fast transport and the calculations give a mean value of 10 K for all time profiles in the full potential simulations. It can reach 30 K if only the harmonic contribution is used. In a translated constant harmonic potential, no modification of the radial internal kinetic energy is observed, showing no coupling between the axial and radial internal motion in this case. Furthermore, if we keep the potential minimum immobile (so that there is no transport) but apply to the trap potential a time variation such that the resulting $\omega_z(t)$ is identical to what is encountered in the moving full potential given by eq.14 (see Fig 4), we observe exactly the same evolution of the internal energy, all along the duration of the transport. This strongly suggests that the deformation of the harmonic part of the axial potential is responsible for the internal heating of the cloud along the transport. This results is consistent with the heating induced in cold atoms due to temporal fluctuations of the harmonic potential secular frequency in the absence of transport [28].

The radial and axial motion of the CM are not directly coupled as the Coulomb interaction plays no role on the CM motion. The radial energy calculated after transport in the full potential is very low compared to the other mentioned energy terms as the largest values (10 mK) are observed for the linear case for any transport duration and for transport faster than 50 μs for the sinus and polynomial profiles, and faster than 200 μs for the tanh case (100 mK). The same characteristic transport durations were already identified in the evolution of the internal axial kinetic energy. Furthermore, if the transport is computed in the harmonic part of the potential, the energy in the radial CM motion remains as low as 0.1 mK for any time profile of any duration, demonstrating that the non-harmonic part of the potential is responsible for this transfer of energy.

Figure 6 shows the transport-induced variation of the internal energy as a function of the initial temperature T_0 for 4 characteristic values : 4 mK, 4 K, 77 K and 300 K. The large relative increase of the internal energy for the coldest sample can be explained by a transfer of Coulomb energy to kinetic energy. This means that, whatever is the initial state of the ion sample, it is in the gaseous phase after the transport, in the explored shuttling protocols.

In this section, we have addressed the energy gain of an ion cloud transported under realistic experimental conditions. This highlights the analogies and discrepancies between the motion of the CM of the cloud and a single ion and the role of the spreading of the cloud for long transport durations in deformed potentials. In the next section, we focus on the other major concern with ion cloud transport : the transport efficiency.

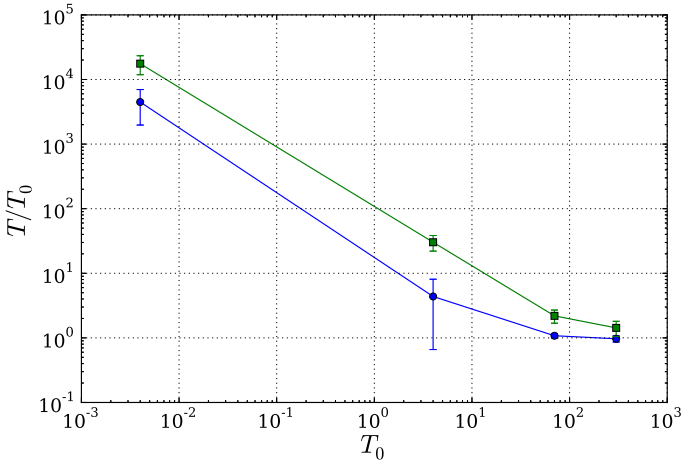

FIG. 6. (Color online) Variation of the internal temperature versus initial temperature for axial (green squares) and radial (blue circles) motion, these values are independent on the transport duration and time-profile.

C. Transport efficiencies

The transport efficiency is defined as the relative number of ions trapped in the destination part of the double trap set-up, once the transport is completed. Lost ions and ions still in the initial part of the trap after the transport protocol are responsible for a lower efficiency. The drastic heating mentioned for very short transport durations does not necessarily induce an ion loss in the potential we simulate, whose depth is approximately 28 eV $= 336 \cdot 10^3 K$ in the axial direction and 9 eV $= 108 \cdot 10^3 K$ in the radial direction. The limits of 100 % efficient transport are shown by the shaded areas in fig 3. Their lower boundaries are due to the inertia of the ions. If the transport is very fast, analysis of the cloud dynamics shows that the ions never leave the first trap, as the potential deformation is too fast for ions to move to the other part of the trap before the central potential barrier is raised again. This behaviour is also observed for a single ion and thus does not depend on the number of trapped ions (see figure 7 for confirmation). The upper boundary for 100% transport is due to the fact that for too long transport duration the ion cloud spreads so much in the axial direction that some ions are still in the initial part of the trap when the central barrier controlled by $V_2(t)$ rises. The comparison between the different curves of figure 3 shows that this limit depends on the minimum time profile and is out of the scale of this figure for the hyperbolic tangent case (N_0=100 ions). As figure 5 shows that the spatial spreading of the cloud increases with the number of ions, a decreasing transfer efficiency is expected for an increasing number of ions. This is confirmed by figure 7 where the number of ions effectively transported to the second part of the trap is plotted for different initial numbers of ions and for the hyperbolic tangent time profile. It shows that for an increasing ion number the limit

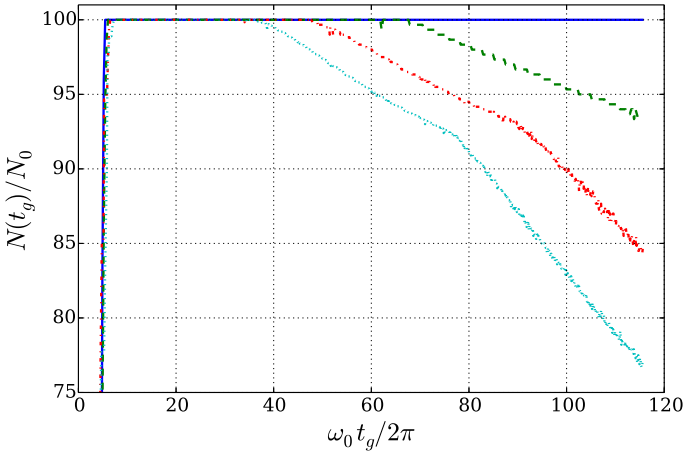

FIG. 7. (Color online) Transport efficiency versus the transport duration t_g in units of $2\pi/\omega_0$, for the hyperbolic tangent profile and different initial ion numbers. The initial internal temperature is ≈ 4 mK in each case. Blue solid line: $N_0 = 100$. Green dashed line: $N_0 = 300$. Red dash-dot line $N_0 = 600$, Cyan dotted line $N_0 = 1000$

transport duration to keep the transport efficiency to 100% decreases. For a given number of ions, the transfer efficiency decreases linearly with the transport duration, showing that the cloud spreading also increases linearly with time. Two different slopes are clearly visible in this evolution, illustrating that a second effect adds to the spreading one. A close analysis of individual dynamics of the ions shows that for the longer transport duration, a second family of ions is found in the first trap : the ones which were ahead and are coming back to the first trap before the barrier is raised. These two effects make long transports between two parts of the same trap not an option, as far as efficiency is concerned. Indeed, the plot of the limit transport duration at which the efficiency is no longer 100% for different ion numbers shows a reduction indicating that for large ion clouds, there may be no transport duration for which 100% of the ions would be shuttled (see figure 8).

IV. CONCLUSION

In conclusion, we have carried out numerical simulations to identify the energy gain source and the cause of reduced efficiency in the shuttling of an ion cloud between the two parts of a linear RF traps separated by 23 mm. This study has been limited to four potential minimum time profiles already studied in the frame of single ion shuttling. The experimental constraints have been reproduced as closely as possible by using trap potentials generated by SIMION. Our transport implementation is limited by the large distance between the electrodes which induces unavoidable deformation of the harmonic potential along the transport. Two causes of transport energy gain are identified. First, the deformation of

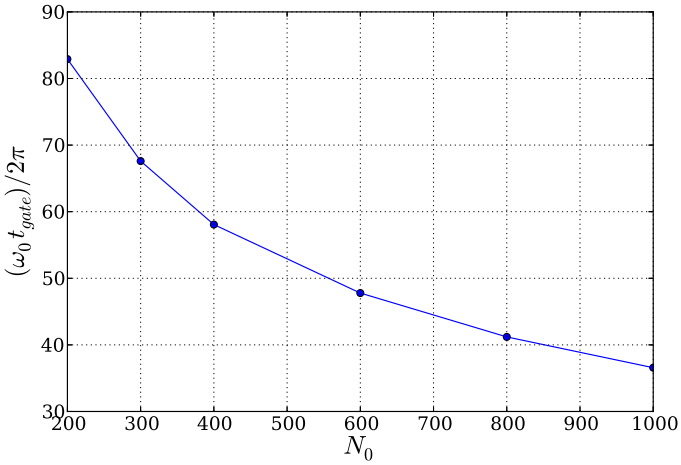

FIG. 8. (Color online) Transport duration t_g at which the transport efficiency is no longer 100% for an hyperbolic tangent profile and different initial ion number N_0.

the harmonic part of the potential is responsible for a large gain in the axial motion kinetic energy of the CM and for the washing out of the periodic energy gain cancellation, except for a linear potential minimum time profile. Such deformations are also responsible for the gain in the kinetic energy in the CM frame for the four studied time profiles. Secondly, because of the cloud's spatial spreading, the non-harmonic components of the potential play an important role in the CM final energy gain for long enough transports, making the use of long transport duration irrelevant for the reduction of the transport-induced energy gain. The spatial spreading is also found to be responsible for the number dependent transfer efficiency reduction observed for longer transport. Nevertheless, simulations show that an efficient (100%) and fast ($200\mu s$) transport of an ion cloud made of more than 1000 ions is still possible at the expense of an energy gain very detrimental for cold ions but irrelevant for clouds with temperatures above 4 K. A challenge is now to design a transport protocol that takes into account the time variation of the secular frequency to reduce the transport induced energy gain.

ACKNOWLEDGMENTS

Scientific discussions with L. Hilico are gratefully acknowledged. This work was partially carried out under ANR grant ANR-08-0053-01. We also acknowledge financial support from

CNES and from Region Provence-Alpes-Côte d'Azur.

---

[1] E. Teloy and D. Gerlich, Chemical Physics **4**, 417 (1974), ISSN 0301-0104, http://www.sciencedirect.com/science/article/pii/0301010474850081

[2] M. W. Senko, C. L. Hendrickson, M. R. Emmett, S. D.-H. Shi, and A. G. Marshall, Journal of the American Society for Mass Spectrometry **8**, 970 (1997), ISSN 1044-0305, http://www.sciencedirect.com/science/article/pii/S1044030597001268

[3] F. Herfurth, Nuclear Instruments and Methods in Physics Research Section B: Beam Interactions with Materials and Atoms **204**, 587 (2003), ISSN 0168-583X, ¡ce:title¿14th International Conference on Electromagnetic Isotope Separators and Techniques Related to their Applications¡/ce:title¿, http://www.sciencedirect.com/science/article/pii/S0168583X02021353

[4] D. Kielpinski, C. Monroe, and D. Wineland, Nature **417**, 709 (2002)

[5] K. Wright, J. M. Amini, D. L. Faircloth, C. Volin, S. Charles Doret, H. Hayden, C.-S. Pai, D. W. Landgren, D. Denison, T. Killian, R. E. Slusher, and A. W. Harter **15**, 033004, ISSN 1367-2630, http://stacks.iop.org/1367-2630/15/i=3/a=033004?key=crossref.2dd5f3491da25e9c8caeae276f2259b1

[6] A. Walther, F. Ziesel, T. Ruster, S. T. Dawkins, K. Ott, M. Hettrich, K. Singer, F. Schmidt-Kaler, and U. Poschinger, Phys. Rev. Lett. **109**, 080501 (Aug 2012), http://link.aps.org/doi/10.1103/PhysRevLett.109.080501

[7] R. Bowler, J. Gaebler, Y. Lin, T. R. Tan, D. Hanneke, J. D. Jost, J. P. Home, D. Leibfried, and D. J. Wineland, Phys. Rev. Lett. **109**, 080502 (Aug 2012), http://link.aps.org/doi/10.1103/PhysRevLett.109.080502

[8] A. Couvert, T. Kawalec, G. Reinaudi, and D. Guéry-Odelin, EPL (Europhysics Letters) **83**, 13001 (Jul. 2008), ISSN 0295-5075, http://iopscience.iop.org/0295-5075/83/1/13001

[9] J.-F. Schaff, X.-L. Song, P. Capuzzi, P. Vignolo, and G. Labeyrie, EPL (Europhysics Letters) **93**, 23001 (2011), http://stacks.iop.org/0295-5075/93/i=2/a=23001

[10] J. Prestage, US Patent 5,420,549(1995), http://www.google.com/patents?hl=en\&lr=\&vid=USPAT5420549\&id=rLgdAAAAEBAJ\&oi=fnd\&dq=%22J+prestage%22\&printsec=abstract

[11] J. Prestage, S. Chung, T. Le, M. Beach, L. Maleki, and R. Tjoelker, Proceedings of 35^{th} Annual Precise Time and Time Interval (PTTI) Meeting(2003), http://tycho.usno.navy.mil/ptti/ptti2003/paper40.pdf

[12] C. Champenois, J. Pedregosa-Gutierrez, M. Marciante, D. Guyomarc'h, M. Houssin, and M. Knoop, AIP Conference Proceedings **1521** (2013)

[13] R. Blümel, J. M. Chen, E. Peik, W. Quint, W. Schleich, Y. R. Shen, and H. Walther, Nature **334**, 309 (1988)

[14] M. Marciante, C. Champenois, A. Calisti, J. Pedregosa-Gutierrez, and M. Knoop, Phys. Rev. A **82**, 033406 (Sep 2010)

[15] Http://www.simion.com

[16] M. Palmero, E. Torrontegui, D. Guéry-Odelin, and J. G. Muga, Phys. Rev. A **88**, 053423 (Nov 2013), http://link.aps.org/doi/10.1103/PhysRevA.88.053423

[17] R. Reichle, D. Leibfried, R. Blakestad, J. Britton, J. Jost, E. Knill, C. Langer, R. Ozeri, S. Seidelin, and D. Wineland, Fortschritte der Physik **54**, 666 (2006), ISSN 1521-3978, http://dx.doi.org/10.1002/prop.200610326

[18] D. Hucul, M. Yeo, S. Olmschenk, C. Monroe, W. K. Hensinger, and J. Rabchuk, Quantum Info. Comput. **8**, 501 (2008), http://dl.acm.org/citation.cfm?id=2016976.2016977

[19] E. Torrontegui, S. Ibáñez, X. Chen, A. Ruschhaupt, D. Guéry-Odelin, and J. G. Muga, Phys. Rev. A **83**, 013415 (Jan 2011), http://link.aps.org/doi/10.1103/PhysRevA.83.013415

[20] H. Dehmelt, Advances in Atomic and Molecular Physics **3**, 53 (1967)

[21] L. Turner, Phys. Fluids **30**, 3196 (1987)

[22] M. Drewsen, C. Brodersen, L. Hornekær, J. S. Hangst, and J. P. Schiffer, Phys. Rev. Lett. **81**, 2878 (1998)

[23] S. Nosé, The Journal of Chemical Physics **81**, 511 (1984), ISSN 0021-9606, 1089-7690, http://scitation.aip.org/content/aip/journal/jcp/81/1/10.1063/1.447334

[24] E. L. Pollock and J. P. Hansen, Phys. Rev. A **8**, 3110 (1973)

[25] R. B. Blakestad, C. Ospelkaus, A. P. Vandevender, J. H. Wesenberg, M. J. Biercuk, D. Leibfried, and D. J. Wineland, Phys. Rev. A **032314**, 1 (2011)

[26] S. Schulz, U. Poschinger, K. Singer, and F. Schmidt-Kaler, Fortschritte der Physik **54**, 648 (2006), ISSN 1521-3978, http://dx.doi.org/10.1002/prop.200610324

[27] K. Singer, U. Poschinger, M. Murphy, P. Ivanov, F. Ziesel, T. Calarco, and F. Schmidt-Kaler, Rev. Mod. Phys. **82**, 2609 (Sep 2010)

[28] M. E. Gehm, K. M. O'Hara, T. A. Savard, and J. E. Thomas, Phys. Rev. A **58**, 3914 (Nov 1998), http://link.aps.org/doi/10.1103/PhysRevA.58.3914